

# ELIQ: A Label-Free Framework for Quality Assessment of Evolving AI-Generated Images

Xinyue Li<sup>1</sup> Zhiming Xu<sup>2</sup> Zhichao Zhang<sup>1</sup> Zhaolin Cai<sup>1</sup> Sijing Wu<sup>1</sup> Xiongkuo Min<sup>1</sup> Yitong Chen<sup>1</sup>  
Guangtao Zhai<sup>1</sup>

## Abstract

Generative text-to-image models are advancing at an unprecedented pace, continuously shifting the perceptual quality ceiling and rendering previously collected labels unreliable for newer generations. To address this, we present **ELIQ**, a *Label-free Framework for Quality Assessment of Evolving AI-generated Images*. Specifically, ELIQ focuses on visual quality and prompt-image alignment, automatically constructs positive and aspect-specific negative pairs to cover both conventional distortions and AIGC-specific distortion modes, enabling transferable supervision without human annotations. Building on these pairs, ELIQ adapts a pre-trained multimodal model into a quality-aware critic via instruction tuning and predicts two-dimensional quality using lightweight gated fusion and a Quality Query Transformer. Experiments across multiple benchmarks demonstrate that ELIQ consistently outperforms existing label-free methods, generalizes from AI-generated content (AIGC) to user-generated content (UGC) scenarios without modification, and paves the way for scalable and label-free quality assessment under continuously evolving generative models. The code will be released upon publication.

## 1. Introduction

The rapid evolution of generative visual models has fundamentally reshaped the perceptual quality landscape of AI-generated content (Cha et al., 2025; Shi et al., 2024). Unlike traditional user-generated content (UGC) images, whose quality distributions are relatively stable (Roy et al., 2023), modern generative models continuously shift the upper bound of perceptual quality within short time spans (Huang

<sup>1</sup>Shanghai Jiao Tong University <sup>2</sup>Xi'an Jiaotong University.  
Correspondence to: Yitong Chen <yitongchen@sjtu.edu.cn>,  
Guangtao Zhai <zhaiguangtao@sjtu.edu.cn>.

Preprint. February 4, 2026.

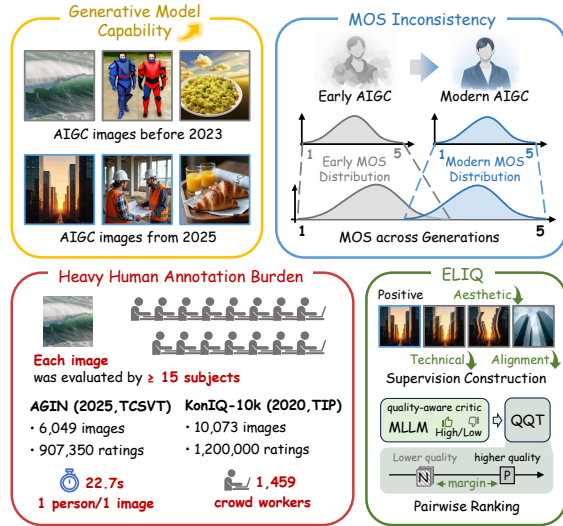


Figure 1. The rapid evolution of generative models shifts MOS distributions, making annotations increasingly inconsistent. ELIQ replaces absolute MOS labels with automatically constructed supervision, enabling scalable quality assessment for evolving AIGC.

et al., 2025). This evolution induces a perceptual drift: artifacts that were once salient become less common, while new failure modes emerge as models change. This implies that evaluation must account for distribution shift and a drifting perceptual reference, rather than assuming a fixed perceptual scale (Hinder et al., 2023).

Current image quality assessment (IQA) methods primarily rely on supervised learning with human mean opinion scores (MOS) (Li et al., 2025; Wang et al., 2024). While MOS can provide reliable subjective judgments under controlled protocols, it implicitly assumes a stable perceptual scale shared across data collection and deployment (Li et al., 2023). This assumption breaks down in rapidly evolving generative settings, as illustrated in Figure 1, where identical MOS values may correspond to markedly different perceptual quality levels across model generations (Hinder et al., 2023). More fundamentally, maintaining valid MOS supervision would require frequent re-annotation to recalibrate the perceptual scale, resulting in limited long-term scalability and heavy annotation cost. As summarized in Table 1, this typically

Table 1. Human annotation scale of representative IQA benchmarks.

Dataset	Images	Human Ratings
KoniQ-10k (Hosu et al., 2020)	10,073	1,208,760
PaQ-2-PiQ (Ying et al., 2019)	40,000	4,000,000
AIGIQA-20K (Li et al., 2024a)	20,000	420,000
AGIN (Chen et al., 2024b)	6,049	907,350
EvalMuse-40k (Han et al., 2024)	40,000	1,000,000
EvalMi-50K (Wang et al., 2025a)	50,400	2,419,200
Q-Eval-100k (Zhang et al., 2025a)	100,000	960,000

requires millions of human ratings even for medium-scale benchmarks.

These limitations have motivated exploration of unsupervised IQA methods, such as NSS-based metrics (Mittal et al., 2012a;b), deep-feature statistics (Ni et al., 2024), reconstruction-based criteria (Shukla et al., 2024), and CLIP-based measures (Wang et al., 2023a). However, most existing approaches are designed for natural images or low-level distortions, and thus transfer poorly to modern AIGC (Peng et al., 2024). In practice, the quality of AI-generated content depends not only on low-level visual fidelity but also on whether the generated image correctly reflects the input prompt and avoids generation-specific artifacts (Peng et al., 2024). Such factors are difficult to capture with conventional unsupervised signals that mainly track low-level statistics. At the same time, although modern large multimodal models (MLLMs) (Wang et al., 2025b; Bai et al., 2025) demonstrate strong visual and semantic understanding, a key open challenge is how to derive scalable and continually updatable supervision that turns MLLMs into reliable label-free evaluators under perceptual drift.

In this work, we propose **ELIQ**, a *Label-free Framework for Quality Assessment of Evolving AI-generated Images*. Our key idea is to replace absolute MOS supervision with automatically constructed relative comparisons that can be periodically refreshed under perceptual drift. ELIQ targets two model-agnostic dimensions of AIGC quality: visual quality and prompt-image alignment. By generating high-quality positives and aspect-aware negative pairs that cover both conventional low-level distortions and AIGC-specific failure modes, ELIQ provides supervision independent of any fixed perceptual scale. Based on this supervision, we fine-tune a pretrained multimodal model into a quality-aware critic, and then train a lightweight scoring module with gated visual-alignment representations and a Quality Query Transformer to predict visual and alignment quality scores.

Experiments on multiple AIGC and UGC benchmarks show that our method consistently outperforms existing unsupervised and label-free approaches and substantially narrows the gap with supervised baselines. Moreover, ELIQ generalizes seamlessly from AIGC to UGC without archi-

tectural modification, providing a scalable alternative to MOS-dependent evaluation and enabling more sustainable quality assessment under evolving generative models. It also generalizes from AIGC to UGC without architecture changes, offering a scalable alternative to MOS-dependent evaluation.

Our main contributions are threefold:

- We introduce **ELIQ**, a label-free framework for quality assessment of evolving AI-generated images, which decouples supervision from fixed MOS scales and remains effective as generative models and perceptual standards evolve.
- We develop an assessment pipeline that jointly models visual quality and prompt-image alignment, using automatically constructed positive and aspect-specific negative pairs to adapt a pretrained multimodal model into a quality-aware critic with lightweight, label-free scoring.
- Extensive experiments across multiple benchmarks show that ELIQ consistently outperforms existing label-free and weakly supervised methods, remains competitive with strong supervised baselines, and generalizes effectively from AI-generated to user-generated image scenarios.

## 2. Related Work

### 2.1. AIGC Generation Models

Recent text-to-image (T2I) models have rapidly evolved with diffusion and transformer-based backbones, continuously raising the perceptual quality ceiling and introducing diverse, model-specific artifacts. Representative advances include DDPM (Ho et al., 2020) and accelerated sampling with DDIM (Song et al., 2021), latent diffusion (Rombach et al., 2022) that underpins Stable Diffusion and SDXL (Podell et al., 2024), and transformer-style diffusion backbones such as DiT (Peebles & Xie, 2023) and PixArt- $\alpha$  (Chen et al., 2024a). Recent large-scale systems further scale data and unified conditioning, e.g., FLUX (Labs et al., 2025) and Qwen-Image (Wu et al., 2025). This fast iteration makes it increasingly difficult to maintain consistent human annotations over time, motivating scalable supervision beyond MOS.

### 2.2. Image Quality Assessment

Early IQA methods estimate perceptual quality using hand-crafted priors such as structural similarity (SSIM) and natural scene statistics (NSS), with representative no-reference metrics including BRISQUE (Mittal et al., 2012a) and NIQE (Mittal et al., 2012b). With deep learning, IQA

shifts to learned quality representations that better handle authentic distortions; transformer-based models such as MUSIQ (Ke et al., 2021) and hybrid designs like MANIQA (Yang et al., 2022) further improve multi-scale context modeling.

### 2.3. Multi-modal Model-based IQA

Vision-language priors enable IQA with stronger semantic awareness and improved zero-shot capability. CLIP-based methods such as LIQE (Zhang et al., 2023) and CLIP-IQA (Wang et al., 2023a) explore embedding alignment and prompt-based assessment for no-reference quality prediction. For AIGC-IQA, several approaches explicitly model prompt-image correspondence, e.g., IPCE (Peng et al., 2024) and CLIP-AGIQA (Fu et al., 2024), while MLLM-based critics have been used to output discrete judgments or continuous scores for both quality and alignment (Zhang et al., 2025b). Despite their progress, most AIGC-IQA methods still rely on large-scale MOS or preference labels, which are costly to refresh under rapidly evolving generative models.

### 2.4. Label-Free IQA Methods

To reduce the dependence on MOS, label-free IQA estimates quality using proxies that avoid human scores. Classical approaches follow an NSS paradigm, measuring deviations from learned pristine statistics, such as NIQE (Mittal et al., 2012b) and IL-NIQE (Zhang et al., 2015). Recent deep variants learn distributional priors or “distance-to-pristine” criteria in feature/latent space (Li et al., 2024b; Shukla et al., 2024; Babu et al., 2023). Another line learns quality-aware representations via self-supervision or pseudo-ranking, including QPT (Zhao et al., 2023), CONTRIQUE (Madhusudana et al., 2022), and ARNIQA (Agnolucci et al., 2024b). Multimodal label-free IQA also emerges, where Quali-CLIP (Agnolucci et al., 2024a) aligns synthetic degradations with quality-related text prompts to learn quality-sensitive embeddings without MOS. However, existing label-free methods often rely on synthetic distortions or proxy supervision, limiting robustness to diverse and model-specific AIGC artifacts and motivating label-free supervision that explicitly constructs quality-aware comparisons.

## 3. Proposed Method

### 3.1. Framework Overview

**Problem setup.** Given an AI-generated image  $I$  and its prompt  $p$ , ELIQ aims to predict two quality scores: a *visual quality* score  $\hat{s}_{\text{vis}}(I)$  and an *alignment quality* score  $\hat{s}_{\text{ali}}(I, p)$ . The key challenge is that MOS-based absolute supervision is expensive and quickly becomes outdated as generative models evolve. ELIQ therefore replaces MOS

with label-free relative supervision that can be re-generated for new model eras.

**Overall pipeline.** ELIQ consists of two coupled components: (i) *Label-Free Supervision Construction* and (ii) *Model Training*. First, we construct a set of high-quality positives and aspect-specific negatives to yield comparison tuples

$$\mathcal{T} = (I^+, I_{\text{tec}}^-, I_{\text{aes}}^-, p, p_{\text{ali}}^-), \quad (1)$$

where  $I_{\text{tec}}^-$  and  $I_{\text{aes}}^-$  degrade visual quality, and  $p_{\text{ali}}^-$  induces prompt-image mismatch. This construction covers both conventional corruptions and AIGC-specific failure modes.

Second, we use these tuples to adapt a pretrained multimodal model into a quality-aware critic and obtain quality scores. Concretely, we (1) perform *quality-aware instruction tuning* to obtain a backbone MLLM $_{\theta^*}$  that can reason about technical quality, aesthetic quality, and alignment, and (2) freeze MLLM $_{\theta^*}$  and train a lightweight scoring module to produce outputs with single-image inference:

$$(I, p) \longrightarrow \hat{s}_{\text{vis}}(I), \hat{s}_{\text{ali}}(I, p). \quad (2)$$

The scoring module is trained only with pairwise ranking constraints derived from  $\mathcal{T}$ , encouraging  $I^+$  to score higher than its visual negatives and  $(I^+, p)$  to score higher than  $(I^+, p_{\text{ali}}^-)$ . With this design, ELIQ remains independent of any fixed MOS scale while directly targeting the two key dimensions of AI-generated image quality.

### 3.2. Label-Free Supervision Construction

#### 3.2.1. PROMPT SELECTION

To cover diverse visual content with clear semantics, we adopt a seven-category taxonomy: Indoor Scenes, Urban Scenes, Natural Scenes, People & Activities, Objects & Artifacts, Food, and Events. Each category is expanded into representative sub-concepts, and we use GPT-5 with category-specific rules to generate 400 text-to-image prompts that are diverse in wording yet consistent in semantics, such as realistic content, category-aligned constraints, and a length limit. Since a prompt may involve multiple concepts, we further assign multi-label categories via a two-step procedure: rule-based keyword matching followed by an LLM refinement for uncertain cases. More details on the taxonomy design, generation rules, and the multi-label assignment are provided in the Appendix.

#### 3.2.2. POSITIVE SAMPLE GENERATION

To construct high-quality positive samples, we use the 400 curated prompts as inputs to three text-to-image generation models: Qwen-Image (Wu et al., 2025), FLUX.1-dev (Labs et al., 2025), and Stable Diffusion 3.5-Large. These prompts cover seven major semantic categories, ensuring representative visual content. These models differ in architecture and

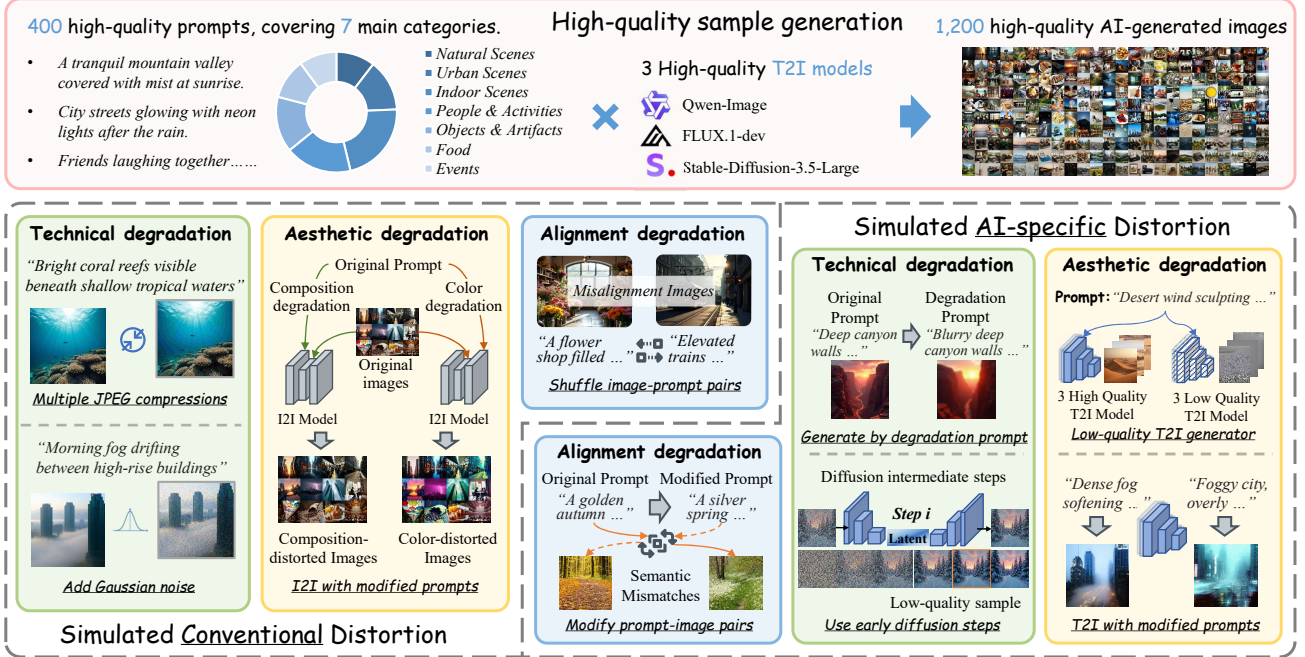


Figure 2. Overview of label-free positive and aspect-specific negative sample construction. High-quality images are generated from curated prompts using multiple T2I models, while negative samples are created by simulating technical, aesthetic, and alignment degradations, including both conventional distortions and AI-specific generation artifacts.

training data, allowing us to obtain image sets that reliably reflect the semantic content described in each prompt. For every prompt, one image is generated by each model, resulting in three corresponding sets of positive samples and a total of 1,200 high-quality AI-generated images.

### 3.2.3. GENERATION OF NEGATIVE SAMPLES

To train our label-free IQA model, we construct diverse negative samples that cover both conventional image corruptions and AIGC-specific failure modes. We design two complementary degradation families, **conventional** and **AI-specific**, each instantiated along three dimensions: **technical**, **aesthetic**, and **alignment** quality.

For conventional degradations, technical negatives are synthesized via repeated JPEG compression and Gaussian noise. Aesthetic negatives are generated by applying controlled image-to-image editing, such as Qwen-Edit (Qwen, 2025) to high-quality images, inducing composition and color degradations while preserving the overall semantic content. Alignment negatives are constructed by shuffling image-prompt pairs, creating semantic mismatches.

For AI-specific degradations, technical negatives are obtained by generating images with explicitly degraded prompts that induce low-fidelity structures, or by prematurely decoding intermediate diffusion latents. Aesthetic negatives are produced via low-quality T2I generation, Stable Diffusion 1.1/1.4/1.5 (CompVis, 2022a;b; RunwayML,

2022), and via prompt modifications that lead to degraded visual appearance. Alignment negatives are constructed by modified prompts to generate images with a high-quality T2I model, followed by mismatching images and prompts across prompt variants to induce semantic misalignment. Detailed generation procedures and settings are provided in the Appendix.

## 3.3. Model Training

Our method contains two stages. First, we perform *Quality-aware Instruction Tuning* to adapt a pretrained MLLM into an aspect-aware backbone. Second, we train a lightweight scoring module, termed *Quality Query Transformer* (QQT), on top of the frozen aspect-aware embeddings. The schematic diagram of the proposed method is shown in Figure 3.

### 3.3.1. QUALITY-AWARE INSTRUCTION TUNING

We adapt a pretrained MLLM into a quality-aware multimodal backbone that can explicitly reason about three perceptual aspects: technical quality, aesthetic quality, and text-image alignment. We formulate each aspect-specific assessment as an instruction-following task and fine-tune the MLLM to output a discrete label low or high. No human MOS annotations are required; instead, we construct supervision using one positive image and aspect-specific negatives generated via controlled degradations.

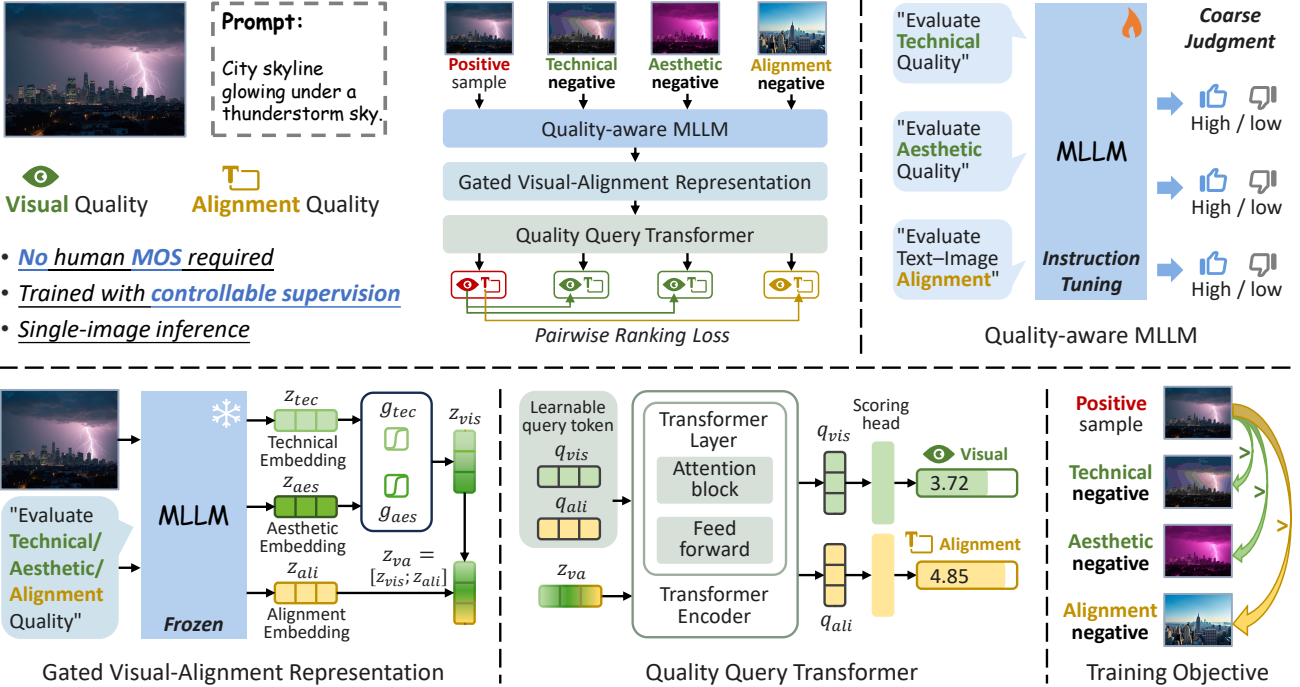


Figure 3. Overview of the proposed label-free visual and alignment quality scoring framework.

**Aspect-specific instructions and negatives.** Given an AIGC image  $I$  and its generation prompt  $p$ , where positive samples  $I^+$  and aspect-specific negatives are constructed following Sec. 3.2.3, we consider

$$d \in \{\text{tec, aes, ali}\}, \quad (3)$$

corresponding to technical quality, aesthetic quality, and semantic alignment, respectively. For each aspect  $d$ , we design an instruction  $\text{instr}_d$  that restricts the model to evaluate only that aspect while ignoring the others. For *technical* and *aesthetic* quality, the instruction does not include the prompt to avoid injecting semantic cues. For *alignment*, the instruction includes the prompt  $p$  as the reference text.

For each positive image  $I^+$ , we synthesize two visually degraded negatives

$$I_{\text{tec}}^-, \quad I_{\text{aes}}^-, \quad (4)$$

where each negative is primarily degraded along its corresponding aspect. For alignment, instead of modifying the image, we construct a mismatched prompt  $p_{\text{ali}}^-$  (e.g., sampled from another instance) and form an alignment-negative pair  $(I^+, p_{\text{ali}}^-)$ .

We assign pseudo-labels such that  $I^+$  is labeled *high* for all three aspects, while  $I_{\text{tec}}^-$  and  $I_{\text{aes}}^-$  are labeled *low* only for their primary aspects, and  $(I^+, p_{\text{ali}}^-)$  is labeled *low* only for alignment. We do not impose supervision on the non-primary aspects because they are not guaranteed by construction.

**Instruction-tuning objective.** We format each query in the standard MLLM chat style. For aspect  $d$ , the input contains the embedded image and  $\text{instr}_d$ ; for  $d = \text{ali}$ , the prompt is included as instructed, while for  $d \in \{\text{tec, aes}\}$  it is omitted. The target response is a single label token  $y_d \in \{\text{low, high}\}$ . Let  $\mathbf{x}_d$  and  $\mathbf{y}_d$  denote the input and output token sequences. We fine-tune the MLLM parameters  $\theta$  by minimizing the autoregressive negative log-likelihood:

$$\mathcal{L}_{\text{SFT}} = -\mathbb{E}_{(\cdot, d)} \left[ \sum_{t=1}^{T_d} \log p_{\theta} (y_{d,t} \mid \mathbf{x}_d, \mathbf{y}_{d,<t}) \right]. \quad (5)$$

After instruction tuning, we freeze the backbone parameters and use it as an aspect-aware feature extractor.

### 3.3.2. GATED VISUAL-ALIGNMENT REPRESENTATION

Discrete *low/high* outputs are too coarse for fine-grained quality prediction. We therefore extract aspect-aware embeddings from the frozen backbone and build a compact representation tailored to two targets: visual quality and alignment quality.

**Frozen aspect-aware embeddings.** Let  $\text{MLLM}_{\theta^*}$  be the instruction-tuned backbone with frozen parameters  $\theta^*$ . For each image  $I$ , we query the backbone with  $\text{instr}_d$  and extract the last-layer hidden state of the final token of input as a continuous embedding. For technical and aesthetic aspects, we omit the prompt:

$$\mathbf{z}_{\text{tec}}(I) = \text{MLLM}_{\theta^*}(I, \text{instr}_{\text{tec}}) \in \mathbb{R}^h, \quad (6)$$

$$\mathbf{z}_{\text{aes}}(I) = \text{MLLM}_{\theta^*}(I, \text{instr}_{\text{aes}}) \in \mathbb{R}^h, \quad (7)$$

and for alignment, we condition on the prompt:

$$\mathbf{z}_{\text{ali}}(I, p) = \text{MLLM}_{\theta^*}(I, p, \text{instr}_{\text{ali}}) \in \mathbb{R}^h, \quad (8)$$

where  $h$  is the backbone hidden size. During training, we obtain alignment-negative embeddings using the mismatched prompt  $p_{\text{ali}}^-$ , i.e.,  $\mathbf{z}_{\text{ali}}(I^+, p_{\text{ali}}^-)$ .

**Gated fusion for visual quality.** Instead of predicting separate technical and aesthetic scores, we fuse their embeddings into a unified visual representation. Given  $\mathbf{z}_{\text{tec}}(I)$  and  $\mathbf{z}_{\text{aes}}(I)$ , we compute two element-wise gates:

$$\mathbf{g}_{\text{tec}} = \sigma(\mathbf{W}_{\text{tec}}[\mathbf{z}_{\text{tec}}; \mathbf{z}_{\text{aes}}]), \quad \mathbf{g}_{\text{aes}} = \sigma(\mathbf{W}_{\text{aes}}[\mathbf{z}_{\text{tec}}; \mathbf{z}_{\text{aes}}]), \quad (9)$$

where  $[\cdot; \cdot]$  denotes concatenation and  $\sigma(\cdot)$  is the sigmoid function. We modulate each branch and produce a fused embedding:

$$\tilde{\mathbf{z}}_{\text{tec}} = \mathbf{z}_{\text{tec}} \odot \mathbf{g}_{\text{tec}}, \quad \tilde{\mathbf{z}}_{\text{aes}} = \mathbf{z}_{\text{aes}} \odot \mathbf{g}_{\text{aes}}, \quad (10)$$

$$\mathbf{z}_{\text{vis}}(I) = \phi([\tilde{\mathbf{z}}_{\text{tec}}; \tilde{\mathbf{z}}_{\text{aes}}]) \in \mathbb{R}^h, \quad (11)$$

where  $\odot$  is element-wise multiplication and  $\phi(\cdot)$  is a small MLP mapping  $\mathbb{R}^{2h} \rightarrow \mathbb{R}^h$ .

### 3.3.3. VISUAL-ALIGNMENT CONCATENATION.

We concatenate the fused visual embedding and the alignment embedding to form the final content token for scoring:

$$\mathbf{z}_{\text{va}}(I, p) = [\mathbf{z}_{\text{vis}}(I); \mathbf{z}_{\text{ali}}(I, p)] \in \mathbb{R}^{2h}. \quad (12)$$

### 3.3.4. QUALITY QUERY TRANSFORMER

We introduce a lightweight Transformer encoder on top of  $\mathbf{z}_{\text{va}}$ , termed Quality Query Transformer (QQT), to predict visual and alignment quality scores. QQT is trained with ranking supervision derived from label-free constructions, while keeping inference strictly single-image. It adopts two learnable query tokens that attend to the content token and extract task-specific evidence for visual and alignment scoring.

Given an input pair  $(I, p)$ , we construct a 3-token sequence

$$\mathbf{X}_3(I, p) = [\mathbf{z}_{\text{va}}(I, p), \mathbf{q}_{\text{vis}}, \mathbf{q}_{\text{ali}}] \in \mathbb{R}^{3 \times 2h}, \quad (13)$$

where  $\mathbf{q}_{\text{vis}}, \mathbf{q}_{\text{ali}} \in \mathbb{R}^{2h}$  are learnable query tokens shared across all samples. We project tokens and add learnable positional embeddings:

$$\mathbf{H}_3(I, p) = \text{TE}(\mathbf{X}_3(I, p) \mathbf{W}_{\text{proj}}^\top + \mathbf{E}_{\text{pos}}) \in \mathbb{R}^{3 \times d_{\text{model}}}, \quad (14)$$

where TE denotes the Transformer encoder. We compute scores by applying two MLP heads,  $f_{\text{vis}}$  and  $f_{\text{ali}}$ , to the corresponding query-token outputs:

$$\hat{s}_{\text{vis}}(I) = f_{\text{vis}}(\mathbf{h}_{\text{vis}}^q(I, p)), \quad \hat{s}_{\text{ali}}(I, p) = f_{\text{ali}}(\mathbf{h}_{\text{ali}}^q(I, p)), \quad (15)$$

where  $\mathbf{h}_{\text{vis}}^q(I, p)$  and  $\mathbf{h}_{\text{ali}}^q(I, p)$  denote the encoded outputs of the visual-query token and alignment-query token in  $\mathbf{H}_3(I, p)$ , respectively.

### 3.3.5. TRAINING OBJECTIVE

We train the gated fusion module and QQT using margin-based ranking losses derived from label-free construction. For each positive pair  $(I^+, p)$ , we construct two visually degraded negatives  $I_{\text{tec}}^-$  and  $I_{\text{aes}}^-$ , and one mismatched prompt  $p_{\text{ali}}^-$  for alignment:

$$\mathcal{T} = (I^+, I_{\text{tec}}^-, I_{\text{aes}}^-, p, p_{\text{ali}}^-). \quad (16)$$

All scores are predicted independently by QQT:

$$\hat{s}_{\text{vis}}(I^+), \hat{s}_{\text{vis}}(I_{\text{tec}}^-), \hat{s}_{\text{vis}}(I_{\text{aes}}^-), \hat{s}_{\text{ali}}(I^+, p), \hat{s}_{\text{ali}}(I^+, p_{\text{ali}}^-). \quad (17)$$

**Visual ranking loss.** Since both  $I_{\text{tec}}^-$  and  $I_{\text{aes}}^-$  are visually degraded, we supervise visual quality with two pairwise constraints (instead of hard-negative aggregation) to avoid gradient sparsity:

$$\begin{aligned} \mathcal{L}_{\text{vis}} = \mathbb{E}_{\mathcal{T}} \Big[ & \max(0, m - \hat{s}_{\text{vis}}(I^+) + \hat{s}_{\text{vis}}(I_{\text{tec}}^-)) \\ & + \max(0, m - \hat{s}_{\text{vis}}(I^+) + \hat{s}_{\text{vis}}(I_{\text{aes}}^-)) \Big]. \end{aligned} \quad (18)$$

**Alignment ranking loss.** For alignment, we enforce that the positive image aligns better with its original prompt than with a mismatched prompt:

$$\mathcal{L}_{\text{ali}} = \mathbb{E}_{\mathcal{T}} \Big[ \max(0, m - \hat{s}_{\text{ali}}(I^+, p) + \hat{s}_{\text{ali}}(I^+, p_{\text{ali}}^-)) \Big]. \quad (19)$$

**Overall objective.** The final loss is

$$\mathcal{L} = \mathcal{L}_{\text{vis}} + \mathcal{L}_{\text{ali}}. \quad (20)$$

### 3.3.6. INFERENCE

Given  $(I, p)$ , we extract frozen embeddings  $\mathbf{z}_{\text{tec}}(I)$ ,  $\mathbf{z}_{\text{aes}}(I)$ , and  $\mathbf{z}_{\text{ali}}(I, p)$ , fuse technical and aesthetic embeddings into  $\mathbf{z}_{\text{vis}}(I)$ , and form  $\mathbf{z}_{\text{va}}(I, p)$ . We then construct  $\mathbf{X}_3(I, p) = [\mathbf{z}_{\text{va}}(I, p), \mathbf{q}_{\text{vis}}, \mathbf{q}_{\text{ali}}]$  and predict two scores:

$$\hat{s}_{\text{vis}}(I), \quad \hat{s}_{\text{ali}}(I, p). \quad (21)$$

Optionally, when a small labeled validation split is available, we apply a monotonic linear calibration to map raw scores to the MOS range. This post-hoc scaling does not affect rank-based evaluation.

Table 2. Performance comparison of ELIQ with supervised, weak-supervised, and label-free methods on three AIGC benchmarks and two UGC benchmarks. The best-performing metric is highlighted in bold, and the second-best is underlined within each supervision setting.

Methods	Type	AIGC Datasets						UGC Datasets			
		AGIQA-3K		AIGCIQA2023		AIGIQA-20K		KonIQ-10k		SPAQ	
		SRCC	PLCC	SRCC	PLCC	SRCC	PLCC	SRCC	PLCC	SRCC	PLCC
<b><i>Supervised</i></b>											
BRISQUE (Mittal et al., 2012a)	handcraft	0.472	0.561	0.446	0.465	0.466	0.558	0.705	0.707	0.802	0.805
HyperIQA (Su et al., 2020)	data-driven	0.850	0.904	0.822	0.852	0.816	0.832	0.904	0.915	0.915	0.918
MANIQA (Yang et al., 2022)	data-driven	0.861	0.911	0.818	0.847	0.850	0.887	0.930	0.946	0.922	0.927
DBCNN (Zhang et al., 2020)	data-driven	0.826	0.890	0.807	0.829	0.805	0.848	0.844	0.862	0.909	0.927
MUSIQ (Ke et al., 2021)	data-driven	0.820	0.865	0.803	0.820	0.832	0.864	0.824	0.937	0.873	0.868
StairIQA (Sun et al., 2023)	data-driven	0.834	0.893	0.808	0.832	0.789	0.842	0.920	0.936	0.923	0.929
Q-Align (Wu et al., 2023)	data-driven	0.852	0.881	0.841	0.860	0.874	0.889	0.922	0.911	0.887	0.886
MA-AGIQA (Wang et al., 2024)	data-driven	0.893	0.927	0.853	0.856	0.864	0.905	0.933	0.948	0.927	0.932
<b><i>Weak-supervised</i></b>											
CONTRIQUE (Madhusudana et al., 2022)	data-driven	0.817	0.879	0.771	0.789	0.788	0.807	0.894	0.906	0.914	0.919
Re-IQA (Saha et al., 2023)	data-driven	0.811	0.874	0.769	0.789	0.787	0.811	<b>0.914</b>	<u>0.923</u>	<b>0.918</b>	<b>0.925</b>
CLIP-IQA+ (Wang et al., 2023a)	data-driven	0.844	0.894	0.817	0.835	0.833	0.854	0.895	0.909	0.864	0.866
ARNIQA (Agnolucci et al., 2024b)	data-driven	0.803	0.881	0.754	0.764	0.778	0.792	0.869	0.883	0.904	0.909
GRepQ-D (Srinath et al., 2024)	data-driven	0.807	0.858	0.767	0.783	0.789	0.810	0.855	0.868	0.903	0.917
<b>Ours</b>	data-driven	<b>0.876</b>	<b>0.911</b>	<b>0.837</b>	<b>0.851</b>	<b>0.856</b>	<b>0.883</b>	<u>0.912</u>	<b>0.924</b>	<u>0.915</u>	<b>0.925</b>
<b><i>Label-free</i></b>											
NIQE (Mittal et al., 2012b)	handcraft	0.523	0.566	0.511	0.523	0.208	0.337	0.551	0.488	0.703	0.670
ILNIQE (Zhang et al., 2015)	handcraft	0.609	0.655	0.594	0.611	0.335	0.455	0.453	0.467	0.719	0.654
CLIP-IQA (Wang et al., 2023a)	data-driven	0.638	0.711	0.589	0.604	0.388	0.537	0.695	0.727	0.738	0.735
MDFS (Ni et al., 2024)	data-driven	0.672	0.676	0.659	0.667	0.691	0.695	0.733	0.737	0.741	0.754
QualiCLIP (Agnolucci et al., 2025)	data-driven	0.667	<u>0.735</u>	0.646	0.661	0.679	0.694	<u>0.817</u>	<b>0.838</b>	<u>0.841</u>	<b>0.851</b>
GRepQ-Z (Srinath et al., 2024)	data-driven	0.613	0.734	0.602	0.612	0.624	0.634	0.768	0.784	0.823	0.839
DUBMA (Wang et al., 2025c)	data-driven	<u>0.684</u>	0.701	<u>0.671</u>	<u>0.680</u>	<u>0.695</u>	<u>0.697</u>	0.703	0.740	0.834	<u>0.841</u>
<b>Ours</b>	data-driven	<b>0.801</b>	<b>0.827</b>	<b>0.767</b>	<b>0.781</b>	<b>0.786</b>	<b>0.803</b>	<b>0.818</b>	<u>0.831</u>	<b>0.842</b>	<b>0.851</b>

## 4. Experiments

### 4.1. Datasets and Experimental Settings

We evaluate our method on three AIGC benchmarks, AGIQA-3K (Li et al., 2023), AIGCIQA2023 (Wang et al., 2023b), and AIGIQA-20K (Li et al., 2024a), as well as two UGC IQA benchmarks, KonIQ-10k (Hosu et al., 2020) and SPAQ (Fang et al., 2020). Details of dataset statistics and splits are provided in the Appendix.

We report performance in two settings. (i) *Label-free*. We directly use the trained model to produce visual and alignment scores without any MOS supervision, and report the correlation with human ratings. (ii) *Weak-supervised*. To measure how well our learned representations transfer to human opinion scores, we append a lightweight linear regressor on the QQT and fine-tune only this linear layer using a small portion of MOS-labeled data (20% for AIGC benchmarks and 30% for UGC benchmarks), while keeping all other modules frozen and evaluating on the remaining dataset.

All experiments are conducted using Qwen3-VL-8B-Instruct as the MLLM backbone. We evaluate the consistency between predicted quality scores  $\{\hat{y}_i\}_{i=1}^N$  and ground-truth scores  $\{y_i\}_{i=1}^N$  using two correlation coefficients:

Spearman’s  $\rho$  (SRCC) and Pearson’s  $r$  (PLCC). More implementation details are provided in the Appendix.

### 4.2. Performance Analysis

The proposed models are trained on the dataset introduced in Section 3.2. The results are summarized in Table 2 for visual quality on both AIGC and UGC benchmarks, and in Table 3 for alignment quality on AIGC benchmarks.

#### 4.2.1. VISUAL QUALITY

In the weak-supervised setting, our method achieves the best performance on all three AIGC benchmarks, with SRCC of 0.876 (AGIQA-3K), 0.837 (AIGCIQA2023), and 0.856 (AIGIQA-20K), remaining competitive with fully supervised approaches. In the *label-free* setting, it consistently outperforms existing label-free and handcrafted baselines, reaching SRCC of 0.801, 0.767, and 0.786 on the same datasets without any target-domain MOS fine-tuning.

On UGC benchmarks, our method attains SRCC of 0.912 on KonIQ-10k and 0.915 on SPAQ using only 30% MOS-labeled data. In contrast, the strongest baseline Re-IQA requires 70% for slightly higher correlation. Without any MOS labels, our label-free variant still achieves SRCC of 0.818 (KonIQ-10k) and 0.842 (SPAQ), demonstrating ro-

Table 3. The performance of the proposed ELIQ method and the compared supervised and label-free alignment quality. The best-performing metric is highlighted in bold.

Methods	AGIQA-3k		AIGCIQA2023	
	SRCC	PLCC	SRCC	PLCC
<b>Weak-supervised</b>				
CLIP (AAAI, 2023)	0.597	0.683	0.617	0.623
CLIP-IQA+ (AAAI, 2023)	0.704	0.738	0.729	0.736
ImageReward (NIPS, 2023)	0.729	0.786	0.749	0.759
HPSv1 (ICCV, 2023)	0.634	0.700	0.663	0.674
PickScore (NIPS, 2023)	0.697	0.763	0.716	0.734
StairReward (TCSVT, 2023)	0.747	0.852	0.760	0.777
IPCE (CVPR, 2024)	0.770	0.872	0.797	0.788
<b>Ours</b>	<b>0.789</b>	<b>0.881</b>	<b>0.804</b>	<b>0.811</b>
<b>Label-free</b>				
CLIP (AAAI, 2023)	0.428	0.450	0.463	0.474
CLIP-IQA+ (AAAI, 2023)	0.501	0.524	0.521	0.538
ImageReward (NIPS, 2023)	0.579	0.607	0.589	0.609
HPSv1 (ICCV, 2023)	0.562	0.577	0.597	0.626
PickScore (NIPS, 2023)	0.593	0.622	0.626	0.652
<b>Ours</b>	<b>0.717</b>	<b>0.730</b>	<b>0.712</b>	<b>0.711</b>

Table 4. Ablation study of the negative degradation we used in ELIQ, where Conv and AI-spec denote Conventional degradation and AI-specific degradation, respectively.

No.	Module		Visual		Alignment	
	Conv	AI-spec	SRCC	PLCC	SRCC	PLCC
1	✓		0.796	0.819	0.713	0.725
2		✓	0.782	0.805	0.702	0.718
3	✓	✓	<b>0.801</b>	<b>0.827</b>	<b>0.717</b>	<b>0.730</b>

bust and scalable quality prediction and effective transfer from AIGC to real-world User-Generated Content.

#### 4.2.2. ALIGNMENT QUALITY

Table 3 presents prompt-image alignment performance on AGIQA-3K and AIGCIQA2023. In the weak-supervised setting, our method achieves the highest correlation on both datasets, while in the label-free setting, it still reaches SRCC of 0.717 on AGIQA-3K and 0.712 on AIGCIQA2023 without using any human annotations, consistently outperforming all label-free baselines.

#### 4.3. Ablation Study

We conduct a set of ablations to validate key components of ELIQ, reporting SRCC and PLCC for both visual quality and alignment quality. We first validated the effectiveness of the degradation of negative samples.

TABLE 4 shows that conventional negatives are more effective than AI-specific ones when used alone, indicating conventional distortion priors provide stable and transferable supervision. Using both together yields the best SRCC

Table 5. Ablation study of the negative degradation we used in ELIQ, where Tec, Aes, and Ali denote technical degradation, aesthetic degradation, and alignment degradation, respectively.

No.	Module			Visual		Alignment	
	Tec	Aes	Ali	SRCC	PLCC	SRCC	PLCC
1	✓			0.773	0.794	0.703	0.712
2		✓		0.769	0.786	0.700	0.711
3			✓	0.751	0.772	0.712	0.723
4	✓	✓		0.789	0.807	0.710	0.719
5		✓	✓	0.787	0.804	0.715	0.727
6	✓		✓	0.796	0.818	0.714	0.728
7	✓	✓	✓	<b>0.801</b>	<b>0.827</b>	<b>0.717</b>	<b>0.730</b>

and PLCC on visual quality and alignment, confirming their complementarity.

TABLE 5 further reveals that a single aspect is insufficient: *Tec*-only/*Aes*-only weakens visual prediction, while *Ali*-only improves alignment but hurts visual quality. Combining two aspects helps, and including *Ali* consistently benefits alignment; the full *Tec+Aes+Ali* setting performs best overall.

In addition, we include four supplementary ablation studies to validate key design choices of ELIQ, as shown in Appendix. Specifically, they examine (i) the necessity of quality-aware instruction tuning for adapting a pretrained MLLM to quality assessment, (ii) the effectiveness of the proposed visual representation that combines technical and aesthetic cues, (iii) the role of the Quality Query Transformer in enabling task-specific quality prediction from a single image, and (iv) the impact of the proposed label-free training objective with multiple ranking constraints.

## 5. Conclusion

Overall, our findings indicate that MLLM-derived quality priors offer a practical and scalable alternative to traditional MOS-based supervision for AIGC quality assessment. Rather than treating quality evaluation as a static, human-anchored problem, our framework reframes it as a model-driven process that can continuously adapt to evolving generative capabilities. This shift opens the door to sustainable quality assessment pipelines that keep pace with rapid advances in generative models, without incurring repeated annotation costs.

## Impact Statement

This paper presents work whose goal is to advance the field of Machine Learning. There are many potential societal consequences of our work, none of which we feel must be specifically highlighted here.

## References

Agnolucci, L., Galteri, L., and Bertini, M. Quality-aware image-text alignment for real-world image quality assessment. *CoRR*, abs/2403.11176, 2024a. URL <https://doi.org/10.48550/arXiv.2403.11176>.

Agnolucci, L., Galteri, L., Bertini, M., and Del Bimbo, A. Arniqa: Learning distortion manifold for image quality assessment. In *2024 IEEE/CVF Winter Conference on Applications of Computer Vision (WACV)*, pp. 188–197, Jan 2024b. doi: 10.1109/WACV57701.2024.00026.

Agnolucci, L., Galteri, L., and Bertini, M. Quality-aware image-text alignment for opinion-unaware image quality assessment, 2025. URL <https://arxiv.org/abs/2403.11176>.

Babu, N. C., Kannan, V., and Soundararajan, R. No reference opinion unaware quality assessment of authentically distorted images. In *2023 IEEE/CVF Winter Conference on Applications of Computer Vision (WACV)*, pp. 2458–2467, Jan 2023. doi: 10.1109/WACV56688.2023.00249.

Bai, S., Cai, Y., Chen, R., Chen, K., Chen, X., Cheng, Z., Deng, L., Ding, W., Gao, C., Ge, C., Ge, W., Guo, Z., Huang, Q., Huang, J., Huang, F., Hui, B., Jiang, S., Li, Z., Li, M., Li, M., Li, K., Lin, Z., Lin, J., Liu, X., Liu, J., Liu, C., Liu, Y., Liu, D., Liu, S., Lu, D., Luo, R., Lv, C., Men, R., Meng, L., Ren, X., Ren, X., Song, S., Sun, Y., Tang, J., Tu, J., Wan, J., Wang, P., Wang, P., Wang, Q., Wang, Y., Xie, T., Xu, Y., Xu, H., Xu, J., Yang, Z., Yang, M., Yang, J., Yang, A., Yu, B., Zhang, F., Zhang, H., Zhang, X., Zheng, B., Zhong, H., Zhou, J., Zhou, F., Zhou, J., Zhu, Y., and Zhu, K. Qwen3-vl technical report. *arXiv preprint arXiv:2511.21631*, 2025.

Cha, J., Ren, M., Singh, K. K., Zhang, H., Hold-Geoffroy, Y., Yoon, S., Jung, H., Yoon, J. S., and Baek, S. Text2relight: Creative portrait relighting with text guidance. *Proceedings of the AAAI Conference on Artificial Intelligence*, 39(2):1980–1988, Apr. 2025. doi: 10.1609/aaai.v39i2.32194. URL <https://ojs.aaai.org/index.php/AAAI/article/view/32194>.

Chen, J., YU, J., GE, C., Yao, L., Xie, E., Wang, Z., Kwok, J., Luo, P., Lu, H., and Li, Z. Pixart-\$\alpha\$: Fast training of diffusion transformer for photorealistic text-to-image synthesis. In *The Twelfth International Conference on Learning Representations*, 2024a. URL <https://openreview.net/forum?id=eAKmQPe3m1>.

Chen, Z., Sun, W., Wu, H., Zhang, Z., Jia, J., Ji, Z., Sun, F., Jui, S., Min, X., Zhai, G., and Zhang, W. Exploring the naturalness of ai-generated images, 2024b. URL <https://arxiv.org/abs/2312.05476>.

CompVis. Stable diffusion v1-1 (compvis/stable-diffusion-v1-1). <https://huggingface.co/CompVis/stable-diffusion-v1-1>, 2022a. Hugging Face model card, accessed 2026-01-02.

CompVis. Stable diffusion v1-4 (compvis/stable-diffusion-v1-4). <https://huggingface.co/CompVis/stable-diffusion-v1-4>, 2022b. Hugging Face model card, accessed 2026-01-02.

Fang, Y., Zhu, H., Zhang, Y., Li, J., and Ma, K. Subjective and objective quality assessment of smartphone photography. In *Proceedings of the IEEE/CVF Conference on Computer Vision and Pattern Recognition (CVPR)*, pp. 1313–1322, 2020.

Fu, J., Zhou, W., Jiang, Q., Liu, H., and Zhai, G. Vision-language consistency guided multi-modal prompt learning for blind ai generated image quality assessment. *IEEE Signal Processing Letters*, 31:1820–1824, 2024. ISSN 1558-2361. doi: 10.1109/LSP.2024.3420083.

Han, S., Fan, H., Fu, J., Li, L., Li, T., Cui, J., Wang, Y., Tai, Y., Sun, J., Guo, C., and Li, C. Evalmuse-40k: A reliable and fine-grained benchmark with comprehensive human annotations for text-to-image generation model evaluation. In *Proceedings of the IEEE/CVF Conference on Computer Vision and Pattern Recognition (CVPR)*, 2024.

Hinder, F., Vaquet, V., Brinkrolf, J., and Hammer, B. Model-based explanations of concept drift. *Neurocomputing*, 555:126640, 2023. ISSN 0925-2312. doi: <https://doi.org/10.1016/j.neucom.2023.126640>. URL <https://www.sciencedirect.com/science/article/pii/S0925231223007634>.

Ho, J., Jain, A., and Abbeel, P. Denoising diffusion probabilistic models. In *Proceedings of the 34th International Conference on Neural Information Processing Systems*, NIPS ’20, Red Hook, NY, USA, 2020. Curran Associates Inc. ISBN 9781713829546.

Hosu, V., Lin, H., Sziranyi, T., and Saupe, D. Koniq-10k: An ecologically valid database for deep learning of blind image quality assessment. *IEEE Transactions on Image Processing*, 29:4041–4056, 2020. ISSN 1941-0042. doi: 10.1109/tip.2020.2967829. URL <http://dx.doi.org/10.1109/TIP.2020.2967829>.

Huang, K., Duan, C., Sun, K., Xie, E., Li, Z., and Liu, X. T2i-compbench++: An enhanced and comprehensive benchmark for compositional text-to-image generation. *IEEE Transactions on Pattern Analysis and Machine Intelligence*, 47(5):3563–3579, 2025. doi: 10.1109/TPAMI.2025.3531907.

Ke, J., Wang, Q., Wang, Y., Milanfar, P., and Yang, F. Musiq: Multi-scale image quality transformer. In *2021 IEEE/CVF International Conference on Computer Vision (ICCV)*, pp. 5128–5137, 2021. doi: 10.1109/ICCV48922.2021.00510.

Labs, B. F., Batifol, S., Blattmann, A., Boesel, F., Consul, S., Diagne, C., Dockhorn, T., English, J., English, Z., Esser, P., Kulal, S., Lacey, K., Levi, Y., Li, C., Lorenz, D., Müller, J., Podell, D., Rombach, R., Saini, H., Sauer, A., and Smith, L. Flux.1 kontext: Flow matching for in-context image generation and editing in latent space, 2025. URL <https://arxiv.org/abs/2506.15742>.

Li, C., Zhang, Z., Wu, H., Sun, W., Min, X., Liu, X., Zhai, G., and Lin, W. Agiqa-3k: An open database for ai-generated image quality assessment. *IEEE Transactions on Circuits and Systems for Video Technology*, pp. 1–1, 2023. doi: 10.1109/TCSVT.2023.3319020.

Li, C., Kou, T., Gao, Y., Cao, Y., Sun, W., Zhang, Z., Zhou, Y., Zhang, Z., Zhang, W., Wu, H., Liu, X., Min, X., and Zhai, G. Aiqqa-20k: A large database for ai-generated image quality assessment. In *Proceedings of the IEEE/CVF Conference on Computer Vision and Pattern Recognition (CVPR) Workshops*, pp. 6327–6336, June 2024a.

Li, Y., Chen, P., Zhu, H., Ding, K., Li, L., and Wang, S. Deep shape-texture statistics for completely blind image quality evaluation. *ACM Trans. Multimedia Comput. Commun. Appl.*, 20(12), November 2024b. ISSN 1551-6857. doi: 10.1145/3694977. URL <https://doi.org/10.1145/3694977>.

Li, Y., Wu, S., Sun, W., Zhang, Z., Zhu, Y., Zhang, Z., Duan, H., Min, X., and Zhai, G. Aghi-qa: A subjective-aligned dataset and metric for ai-generated human images, 2025. URL <https://arxiv.org/abs/2504.21308>.

Madhusudana, P. C., Birkbeck, N., Wang, Y., Adsumilli, B., and Bovik, A. C. Image quality assessment using contrastive learning. *IEEE Transactions on Image Processing*, 31:4149–4161, 2022. ISSN 1941-0042. doi: 10.1109/TIP.2022.3181496.

Mittal, A., Moorthy, A. K., and Bovik, A. C. No-reference image quality assessment in the spatial domain. *IEEE Transactions on image processing*, 21(12):4695–4708, 2012a.

Mittal, A., Soundararajan, R., and Bovik, A. C. Making a “completely blind” image quality analyzer. *IEEE Signal processing letters*, 20(3):209–212, 2012b.

Ni, Z., Liu, Y., Ding, K., Yang, W., Wang, H., and Wang, S. Opinion-unaware blind image quality assessment using multi-scale deep feature statistics. *IEEE Transactions on Multimedia*, 26:10211–10224, 2024. ISSN 1941-0077. doi: 10.1109/TMM.2024.3405729.

Peebles, W. and Xie, S. Scalable diffusion models with transformers. In *Proceedings of the IEEE/CVF international conference on computer vision*, pp. 4195–4205, 2023.

Peng, F., Fu, H., Ming, A., Wang, C., Ma, H., He, S., Dou, Z., and Chen, S. AIGC Image Quality Assessment via Image-Prompt Correspondence . In *2024 IEEE/CVF Conference on Computer Vision and Pattern Recognition Workshops (CVPRW)*, pp. 6432–6441, Los Alamitos, CA, USA, June 2024. IEEE Computer Society. doi: 10.1109/CVPRW63382.2024.00644. URL <https://doi.ieee.org/10.1109/CVPRW63382.2024.00644>.

Podell, D., English, Z., Lacey, K., Blattmann, A., Dockhorn, T., Müller, J., Penna, J., and Rombach, R. SDXL: Improving latent diffusion models for high-resolution image synthesis. In *The Twelfth International Conference on Learning Representations*, 2024. URL <https://openreview.net/forum?id=di52zR8xgf>.

Qwen. Qwen-image-edit (qwen/qwen-image-edit). <https://huggingface.co/Qwen/Qwen-Image-Edit>, 2025. Model card, accessed 2026-01-02.

Rombach, R., Blattmann, A., Lorenz, D., Esser, P., and Ommer, B. High-resolution image synthesis with latent diffusion models. In *Proceedings of the IEEE/CVF conference on computer vision and pattern recognition*, pp. 10684–10695, 2022.

Roy, S., Mitra, S., Biswas, S., and Soundararajan, R. Test time adaptation for blind image quality assessment. In *Proceedings of the IEEE/CVF International Conference on Computer Vision*, pp. 16742–16751, 2023.

RunwayML. Stable diffusion v1-5 (runwayml/stable-diffusion-v1-5; mirrored). <https://huggingface.co/stable-diffusion-v1-5/stable-diffusion-v1-5>, 2022. Hugging Face model card (mirror of deprecated runwayml repository), accessed 2026-01-02.

Saha, A., Mishra, S., and Bovik, A. C. Re-iqa: Unsupervised learning for image quality assessment in the wild. In *2023 IEEE/CVF Conference on Computer Vision and Pattern Recognition (CVPR)*, pp. 5846–5855, June 2023. doi: 10.1109/CVPR52729.2023.00566.

Shi, J., Gao, P., and Qin, J. Transformer-based no-reference image quality assessment via supervised contrastive learning. *Proceedings of the AAAI Conference on Artificial*

*Intelligence*, 38(5):4829–4837, Mar. 2024. doi: 10.1609/aaai.v38i5.28285. URL <https://ojs.aaai.org/index.php/AAAI/article/view/28285>.

Shukla, A., Upadhyay, A., Bhugra, S., and Sharma, M. Opinion unaware image quality assessment via adversarial convolutional variational autoencoder. In *2024 IEEE/CVF Winter Conference on Applications of Computer Vision (WACV)*, pp. 2142–2152, Jan 2024. doi: 10.1109/WACV57701.2024.00215.

Song, J., Meng, C., and Ermon, S. Denoising diffusion implicit models. In *International Conference on Learning Representations*, 2021. URL <https://openreview.net/forum?id=St1giarCHLP>.

Srinath, S., Mitra, S., Rao, S., and Soundararajan, R. Learning generalizable perceptual representations for data-efficient no-reference image quality assessment. In *Proceedings of the IEEE/CVF Winter Conference on Applications of Computer Vision (WACV)*, pp. 22–31, January 2024.

Su, S., Yan, Q., Zhu, Y., Zhang, C., Ge, X., Sun, J., and Zhang, Y. Blindly assess image quality in the wild guided by a self-adaptive hyper network. In *2020 IEEE/CVF Conference on Computer Vision and Pattern Recognition (CVPR)*, pp. 3664–3673, June 2020. doi: 10.1109/CVPR42600.2020.00372.

Sun, W., Min, X., Tu, D., Ma, S., and Zhai, G. Blind quality assessment for in-the-wild images via hierarchical feature fusion and iterative mixed database training. *IEEE Journal of Selected Topics in Signal Processing*, 2023.

Wang, J., Chan, K. C., and Loy, C. C. Exploring clip for assessing the look and feel of images. *Proceedings of the AAAI Conference on Artificial Intelligence*, 37(2): 2555–2563, Jun. 2023a. doi: 10.1609/aaai.v37i2.25353.

Wang, J., Duan, H., Liu, J., Chen, S., Min, X., and Zhai, G. Aigcqa2023: A large-scale image quality assessment database for ai generated images: from the perspectives of quality, authenticity and correspondence. In *CAAI International Conference on Artificial Intelligence*, pp. 46–57. Springer, 2023b.

Wang, J., Duan, H., Zhao, Y., Wang, J., Zhai, G., and Min, X. Lmm4lmm: Benchmarking and evaluating large-multimodal image generation with lmms. In *Proceedings of the IEEE/CVF International Conference on Computer Vision (ICCV)*, pp. 17312–17323, October 2025a.

Wang, P., Sun, W., Zhang, Z., Jia, J., Jiang, Y., Zhang, Z., Min, X., and Zhai, G. Large multi-modality model assisted ai-generated image quality assessment. In *Proceedings of the 32nd ACM International Conference on Multimedia, MM '24*, pp. 7803–7812, New York, NY, USA, 2024. Association for Computing Machinery. ISBN 9798400706868. doi: 10.1145/3664647.3681471. URL <https://doi.org/10.1145/3664647.3681471>.

Wang, W., Gao, Z., Gu, L., Pu, H., Cui, L., Wei, X., Liu, Z., Jing, L., Ye, S., Shao, J., et al. Internvl3.5: Advancing open-source multimodal models in versatility, reasoning, and efficiency. *arXiv preprint arXiv:2508.18265*, 2025b.

Wang, Z., Liu, X., Yan, J., Wen, J., Wang, W., and Huang, C. Deep opinion-unaware blind image quality assessment by learning and adapting from multiple annotators. In *Proceedings of the Thirty-Fourth International Joint Conference on Artificial Intelligence, IJCAI-25*, pp. 2036–2044, 2025c.

Wu, C., Li, J., Zhou, J., Lin, J., Gao, K., Yan, K., ming Yin, S., Bai, S., Xu, X., Chen, Y., Chen, Y., Tang, Z., Zhang, Z., Wang, Z., Yang, A., Yu, B., Cheng, C., Liu, D., Li, D., Zhang, H., Meng, H., Wei, H., Ni, J., Chen, K., Cao, K., Peng, L., Qu, L., Wu, M., Wang, P., Yu, S., Wen, T., Feng, W., Xu, X., Wang, Y., Zhang, Y., Zhu, Y., Wu, Y., Cai, Y., and Liu, Z. Qwen-image technical report, 2025. URL <https://arxiv.org/abs/2508.02324>.

Wu, H., Zhang, Z., Zhang, W., Chen, C., Liao, L., Li, C., Gao, Y., Wang, A., Zhang, E., Sun, W., et al. Q-align: Teaching lmms for visual scoring via discrete text-defined levels. *arXiv preprint arXiv:2312.17090*, 2023.

Yang, S., Wu, T., Shi, S., Lao, S., Gong, Y., Cao, M., Wang, J., and Yang, Y. MANIQA: Multi-dimension Attention Network for No-Reference Image Quality Assessment. In *2022 IEEE/CVF Conference on Computer Vision and Pattern Recognition Workshops (CVPRW)*, pp. 1190–1199, Los Alamitos, CA, USA, June 2022. IEEE Computer Society. doi: 10.1109/CVPRW56347.2022.00126. URL <https://doi.ieee.org/10.1109/CVPRW56347.2022.00126>.

Ying, Z., Niu, H., Gupta, P., Mahajan, D., Ghadiyaram, D., and Bovik, A. From patches to pictures (paq-2-piq): Mapping the perceptual space of picture quality, 2019. URL <https://arxiv.org/abs/1912.10088>.

Zhang, L., Zhang, L., and Bovik, A. C. A feature-enriched completely blind image quality evaluator. *IEEE Transactions on Image Processing*, 24(8):2579–2591, Aug 2015. ISSN 1941-0042. doi: 10.1109/TIP.2015.2426416.

Zhang, W., Ma, K., Yan, J., Deng, D., and Wang, Z. Blind image quality assessment using a deep bilinear convolutional neural network. *IEEE Transactions on Circuits and Systems for Video Technology*, 30(1):36–47, 2020. doi: 10.1109/TCSVT.2018.2886771.

Zhang, W., Zhai, G., Wei, Y., Yang, X., and Ma, K. Blind image quality assessment via vision-language correspondence: A multitask learning perspective. In *Proceedings of the IEEE/CVF Conference on Computer Vision and Pattern Recognition (CVPR)*, pp. 14071–14081, June 2023.

Zhang, Z., Kou, T., Wang, S., Li, C., Sun, W., Wang, W., Li, X., Wang, Z., Cao, X., Min, X., Liu, X., and Zhai, G. Q-eval-100k: Evaluating visual quality and alignment level for text-to-vision content. In *Proceedings of the IEEE/CVF Conference on Computer Vision and Pattern Recognition (CVPR)*, 2025a.

Zhang, Z., Li, X., Sun, W., Zhang, Z., Li, Y., Liu, X., and Zhai, G. Leveraging multimodal large language models for joint discrete and continuous evaluation in text-to-image alignment. In *Proceedings of the IEEE/CVF Conference on Computer Vision and Pattern Recognition (CVPR) Workshops*, pp. 977–986, June 2025b.

Zhao, K., Yuan, K., Sun, M., Li, M., and Wen, X. Quality-aware pretrained models for blind image quality assessment. In *2023 IEEE/CVF Conference on Computer Vision and Pattern Recognition (CVPR)*, pp. 22302–22313, June 2023. doi: 10.1109/CVPR52729.2023.02136.